

Article

Extreme Floods in Small Mediterranean Catchments: Long-Term Response to Climate Variability and Change

Gerardo Benito ^{1,*}, Yolanda Sanchez-Moya ², Alicia Medialdea ³, Mariano Barriendos ⁴, Mikel Calle ¹, Mayte Rico ⁵, Alfonso Sopena ⁶ and Maria J. Machado ¹

¹ Department of Geology, National Museum of Natural Sciences (MNCN), CSIC, Serrano 115 bis, 28006 Madrid, Spain; m.calle@mncn.csic.es (M.C.); machado@mncn.csic.es (M.J.M.)

² Facultad CC. Geológicas, Universidad Complutense de Madrid-Instituto de Geociencias (CSIC-Universidad Complutense de Madrid), 28006 Madrid, Spain; yol@ucm.es

³ Institute of Geography, University of Cologne, 50674 Cologne, Germany; amediald@uni-koeln.de

⁴ Department of History and Archaeology, University of Barcelona, Montalegre 6, 08001 Barcelona, Spain; barriendos@telefonica.net

⁵ Pyrenean Institute of Ecology (IPE-CSIC), Avda Montañana 1005, 50059 Zaragoza, Spain; mayterico68@gmail.com

⁶ Instituto de Geociencias (CSIC-Universidad Complutense de Madrid), 28006 Madrid, Spain; sopena@ucm.es

* Correspondence: benito@mncn.csic.es; Tel.: +34-917-822-083

Received: 2 March 2020; Accepted: 27 March 2020; Published: 1 April 2020



Abstract: Climate change implies changes in the frequency and magnitude of flood events. The influence of climate variability on flooding was evaluated by an analysis of sedimentary (palaeofloods) and documentary archives. A 500-year palaeoflood record at Montlleó River (657 km² in catchment area), eastern Spain, revealed up to 31 palaeofloods with a range of discharges of 20–950 m³ s⁻¹, and with at least five floods exceeding 740–950 m³ s⁻¹. This information contrasts with the available gauged flood registers (since year 1971) with an annual maximum daily discharge of 129 m³ s⁻¹. Our palaeoflood dataset indicates flood cluster episodes at (1) 1570–1620, (2) 1775–1795, (3) 1850–1890, and (4) 1920–1969. Flood rich periods 1 and 3 corresponded to cooler than usual (about 0.3 °C and 0.2 °C) climate oscillations, whereas 2 and 4 were characterised by higher inter-annual climatic variability (floods and droughts). This high inter-annual rainfall variability increased over the last 150 years, leading to a reduction of annual maximum flow. Flood quantiles (>50 years) calculated from palaeoflood+gauged data showed 30%–40% higher peak discharges than those using only instrumental records, whereas when increasing the catchment area (1500 km²) the discharge estimation variance decreased to ~15%. The results reflect the higher sensitivity of small catchments to changes on flood magnitude and frequency due to climate variability whereas a larger catchment buffers the response due to the limited extent of convective storms. Our findings show that extended flood records provide robust knowledge about hazardous flooding that can assist in the prioritization of low-regret actions for flood-risk adaptation to climate change.

Keywords: palaeofloods; floods; climate change; flood frequency; climate change adaptation; Mediterranean rivers; Spain

1. Introduction

Global warming is leading to widespread changes in the hydrological cycle although the chain linking greenhouse gases to outcome impacts is long and complex [1]. A more variable climate and therefore, a more variable water cycle is likely to affect the pattern of rainfall-producing floods [2].

To date, widespread observations of changes in flood magnitude or frequency due to anthropogenic climate change are not widely available [1]. There is, however, a growing public awareness of the increase in flood activity caused by a growing number of reported floods worldwide [3]. Three possible factors explain this increase in flood risk perception: higher population exposure, higher vulnerability, and higher frequency and/or intensity of hazard [4]. Yet, the specific weight of each of these factors included in the flood risk equation is still under debate.

In the Iberian Mediterranean region, climate model projections for extreme rainfall (RCP 4.5 and RCP 8.5) estimate changes of both decrease and increase quantiles, ranging from -20% to $+15\%$ for the 10-year return time and -20% to $+25\%$ for the 100-year return period [5,6]. At European scale, flood projections based on EURO-CORDEX data show even higher uncertainties for 100-year flood discharges [7]. Observed flood peaks from gauged records (1942–2009) fail to show a well-defined trend over the Mediterranean Spanish catchments [8] but for the evidence of a shift towards later seasonal floods [9]. The lack of significant statistical connection between climate change and changes in flood hazards is explained by the high inter-annual variability of extreme events and short stream gauge data series [3]. Moreover, land use changes and river regulation by dams have obscured the detection of climate-driven changes to floods [10]. A long-term flood-climate perspective is urged to improve our understanding of modern flood hazards and regional changes under a warming climate.

In recent decades, geomorphological and sedimentary indicators have been used to quantify flood discharge and frequency over centennial-to-millennia time scales with applications for engineering design and risk estimation [11,12]. Palaeoflood sedimentary indicators provide long-lasting evidence of peak flow stages, and typically consist of fine-textured sediment layers within vertically stacked depositional sequences accumulated at valley sides, known as slack-water flood deposits [13]. This palaeoflood archive provides physical evidence on the natural persistence of flooding, range of magnitude, and response to atmospheric circulation [14,15]. The understanding of hydrological response to environmental history contributes to the assessment of changes in the flood patterns linked to anthropogenic global change [3,16,17].

This paper presents recent advances in the use of palaeoflood data in order to improve our understanding of flood hazard changes under climate variability in small Mediterranean catchments. The following sections elaborate on some key research questions on the influence of climate change on floods, and how palaeoflood hydrology contributes to understand, predict and improve flood hazard assessment. The specific objectives were: (1) the analysis of spatial and temporal pattern of flood frequency to assess relations among climate, land-use and geomorphic response; (2) the assessment of recent flood magnitudes in the context of past flood events based on a case study of a small Mediterranean river catchment, (3) the appraisal of the contributions of palaeoflood hydrology to improve frequency analysis, and (4) the assessment of the maximum limit of flood magnitude and non-exceedances as a criterion of maximum floods estimated by deterministic and stochastic models in small watersheds.

2. Study Area

The Montlleó River (657 km² in catchment area) is one of the three major tributaries of Rambla de la Viuda (1500 km²), a large ephemeral Mediterranean catchment located in eastern Spain (Figure 1). The catchment headwater is on the Iberian Range at 1600 m a.s.l., cutting along its course a sinuous bedrock channel on Mesozoic limestones and on well-cemented Tertiary gravels. Our palaeoflood study was carried out in a 500-m reach (00°06′57.10″ W; 40°14′07.00″ N) located 6 km upstream of its confluence with Rambla Carbonera.

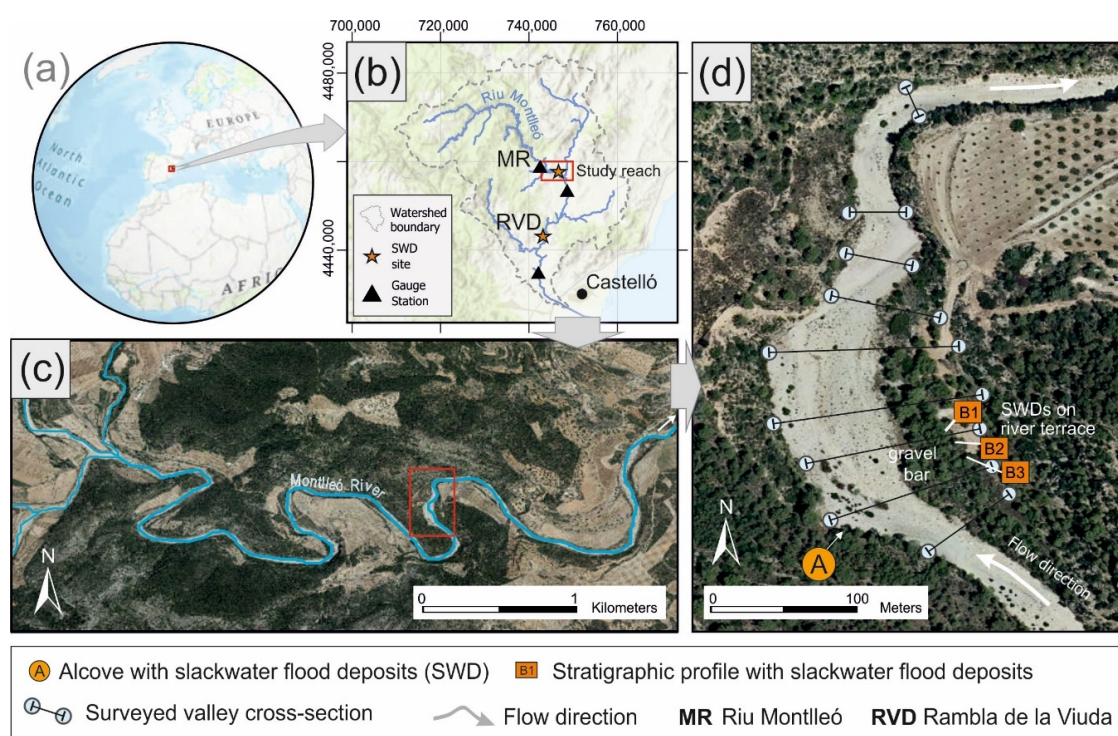


Figure 1. (a) The Montlleó River in the Iberian Peninsula. (b): Location of the Montlleó River in the Rambla de la Viuda River (RVD) catchment in eastern Spain. (c) Aerial photo of the Montlleó stream channel constrained laterally by bedrock, and location of the reach preserving slackwater flood deposits (SWD). (d) Study reach illustrating the location of slackwater flood deposits overlying a stream terrace (square B#) and in a rock alcove (circled A), and surveyed cross sections used in the hydraulic model.

The climate is meso-mediterranean at the upper catchment (pine and evergreen oak forests) to thermo-mediterranean (shrublands) in most of the basin, characterised by a mean annual temperature of 9–15 °C, daily winter minima easily below 0 °C and summer maxima above 30 °C. Mean annual precipitation ranges from over 750 mm in Peñagolosa peak to 500 mm in the lower catchment [18]. Rainfall occurs mainly in autumn (September to November), with a second rainfall maximum in late winter to spring (March to May). The most intense rainfall episodes (up to 300 mm in 24 h) occur in autumn, associated to mesoscale convective cells [19], leading to extreme flooding in the region [20].

In the study reach, locally known as La Volta (The Tour), the valley is constrained laterally by bedrock and the channel bed is built on alluvial gravel (Figure 1). The lower sector is narrow (20-m in width) and expands upstream (60–70 m in width) which favours sedimentation during flood events. The analysis of the fluvial morphodynamic changes based on aerial photographs (1946–2017), supported by field check-up, indicates that some channel bed incision occurred mainly since 1976, when in-stream gravel mining started [21,22]. The uncertainty regarding the valley geometry at the time of the deposition of the slackwater flood deposits was considered in the hydraulic modelling as a possible range of channel topography and discharge.

3. Materials and Methods

3.1. Palaeoflood Record

Quantitative palaeoflood hydrology methods were used to estimate the magnitude and frequency of past flooding on bases of sedimentary evidence [23]. Fine sediments in suspension are accumulated in slackwater depositional environments, such as channel widening, alcoves and caves in bedrock walls, and back-flooded tributary mouths [12,13]. In these sites, sequences of multiple sedimentation layers record multiple flood events, sometimes with intercalated slope deposits, or with contacts marked

by unconformities [13]. A detailed stratigraphy with emphasis on contacts between flood-related sediment beds was performed in 8 stratigraphic profiles, along with a stratigraphic panel of the main outcrop with lateral changes of flood layer contacts and unconformities. In these stratigraphic profiles (B1, B2, etc.; Figure 1) particular attention was given to the identification of individual flood layers (unit number; Unit #), texture, colour, organic remnants for age dating (Table 1) and sedimentary flow structures [24]. The stratigraphy was completed with a trench, dug on the inner alcove infill (close to its end), as well as on remnants of high SWD sediments attached to the alcove walls. At selected sites, sediment peels of the stratigraphic profiles, measuring approximately 80 cm × 50 cm in size, were made in the field [25].

Table 1. Radiocarbon dating with indication of stratigraphic profile and unit number.

Profile/#Flood Unit	Sample Material	Lab Code (Field Code) ¹	Age, ¹⁴ C Years BP	Calibrated Age Range ² , CE 95.4% Probability	Most Likely Age Range, CE
B2 #Bsd4	Charcoal 13C/12C: −24.7‰	Beta-299037 (B2-4-3)	130 ± 30	1674–1778 (38.0%) 1798–1894 (42.4%) 1905–1942 (14.9%)	1798–1894
MLL #1	Charcoal δ13C: −30.74 ± 1.1‰	CNA1416 (ML-5)	135 ± 30	1672–1778 (40.8%) 1799–1892 (39.6%) 1907–1953 (15%) 1660–1700 (18%)	1672–1778
MLL #12	Charcoal δ13C: −24.05 ± 0.9‰	CNA1417 (ML-1-37)	170 ± 30	1720–1820 (52%) 1833–1881 (10%) 1915–1953 (20%)	1720–1820
MLL #17	Charcoal δ13C: −27.5 ± 0.95‰	CNA1418 (ML1)	125 ± 30	1677–1765 (35%) 1800–1896 (47%) 1902–1953 (17%)	1800–1896
MLR #15D	Charcoal δ13C: −27.4 ± 1.2‰	CNA1419 (ML3)	185 ± 30	1650–1694 (22%) 1726–1813 (57%) 1853–1867 (1%) 1918–1952 (20%)	1726–1813
AML1 #1	Charcoal 13C/12C: −22.3‰	Beta-299038 (AML-T1)	50 ± 30	1694–1728 (21.8%) 1812–1919 (73.6%)	1694–1728
AML1 #2	Charcoal	Poz-42337 (AML-T2)	195 ± 30	1648–1690 (23.1%) 1728–1810 (52.3%) 1925–... (20.0%)	1728–1810
AML1 #3	Charcoal 13C/12C: −25.8‰	Beta-299039 (AML-T3)	80 ± 30	1690–1730 (24.9%) 1810–1926 (70.5%)	1810–1926
AML2 #7	Charcoal 13C/12C: −25.5‰	Beta-299040 (AML2-7)	70 ± 30	1690–1730 (24.3%) 1810–1924 (71.1%)	1810–1924

¹ The laboratory code refers to the following radiocarbon dating facilities: CNA: Spanish Accelerator Centre in Seville; Poz: Poznan Radiocarbon Laboratory; Beta: Radiocarbon service of Beta Analytic. ² Radiocarbon ages were calibrated to calendar ages. Some conventional ¹⁴C BP dates have multiple intercepts in the calendar year BP curve. Two Sigma calibrated age is provided in ranges with indication of their relative area (in %) under 2σ distribution.

3.2. Palaeoflood Dating

The age of the palaeoflood events was determined using radiocarbon and optically stimulated luminescence (OSL) dating of samples collected from individual flood units. Radiocarbon AMS analyses were carried out at three laboratories: (1) Spanish Accelerator Centre in Seville (CNA), (2) Poznan Radiocarbon Laboratory (Poz) and (3) Radiocarbon service of Beta Analytic in Florida (Beta). Radiocarbon dates are quoted in the text as the two-sigma calibrated age range (95%). Radiocarbon ages were calibrated to calendar ages by Oxcal 4.3 software [26] based on IntCal 13 [27] calibration data set (Table 1). Luminescence measurements were carried out in two laboratories: (1) the Nordic Laboratory for Luminescence Dating in Denmark, and (2) the Radioisotopes Unit at the University of Seville.

Luminescence dating determines the time elapsed since quartz and feldspar grains were last exposed to daylight [28,29]. For purposes of dating flood deposits, the general assumption is that the sediment was last exposed to daylight (bleached) during transport prior deposition. The OSL dating was completed for a total of 8 sand samples (Table 2) collected in the field using PVC cylinders to avoid exposure of the sediment to white light. In these sand samples, quartz grains of size 180–250 μm were extracted under light-controlled conditions for luminescence measurements. This grain size has been selected as it has shown to be better bleached than smaller grain sizes [30]. In addition, when measured in small aliquots (<30 grains per aliquot), it provides enough resolution on dose to identify incomplete bleaching (insufficient exposure to daylight to reset the luminescence signal during transport) of the sediment [29,30]. A preheat temperature of 200 °C for 10 s and a cut-heat of 180 °C at a heating rate of 5 °C/s was used for all measurements. A dose recovery experiment has shown that this temperature combination does not derive in thermal transfer. In total, 40–60 aliquots of 2 mm (~20 grains each aliquot) have been measured for each sample to generate the corresponding dose distributions. Individual equivalent doses (De) were determined by interpolating the natural luminescence signal into the dose response curved defined using the single aliquot regenerative dose (SAR) protocol [31].

Table 2. Results from optically stimulated luminescence dating applied to eight slackwater flood deposits in Montlleó. The last column of this table shows the ages converted to CE/BCE to facilitate the comparison with the rest of ages reported in the manuscript.

Profile/Flood Unit#	Depth (cm)	Age (Years b. 2013)	Equivalent Dose (Gy)	Dose Rate (Gy/ka) ¹	Age CE/BCE
MLL #2	3.80	0.39 ± 0.03	0.45 ± 0.03	1.15 ± 0.04	1593–1653
MLL #8	2.80	0.45 ± 0.05	0.52 ± 0.06	1.16 ± 0.04	1513–1613
MLL #13	1.90	0.60 ± 0.08	0.56 ± 0.07	0.93 ± 0.04	1333–1493
MLL #17	1.40	1.6 ± 0.1	1.9 ± 0.1	1.15 ± 0.04	313–513
MLR #10	2.50	0.49 ± 0.08	0.38 ± 0.06	0.78 ± 0.03	1443–1603
AML1 #1	0.70	0.47 ± 0.07	0.58 ± 0.08	1.24 ± 0.04	1473–1613
B1 #3	0.45	4.0 ± 0.2	4.3 ± 0.1	1.07 ± 0.04	BCE 2187–1787
B1 #4	0.65	4.6 ± 0.2	4.2 ± 0.1	0.92 ± 0.04	BCE 2787–2387

¹ Total dose rates were calculated from radionuclide activity concentration plus the contribution of cosmic radiation according to the burial depth. Estimated OSL ages are reported in years before 2013 (sampling date).

The measurements included a step with infrared stimulation to detect the presence of feldspar [32], which could compromise the reliability of the detected signal assumed to generate from quartz. Burial De for each sample was estimated using the Internal-External Consistency Criteria (IEU) approach [33,34] proposed to identify the population of doses most likely to correspond to well bleached grains. The parameters needed for the IEU approach are based on an ideal dose distribution only affected by intrinsic factors, therefore excluding the effect of incomplete bleaching. Such “ideal” dose distribution was generated by bleaching a subsample of sample MLL-17 and irradiating it with a known dose. The derived dose distribution was characterized by an over-dispersion of 15%.

The annual dose rates are based on the radionuclide activity concentration measured on ~200 g of bulk material using high resolution gamma spectrometry. Contribution of cosmic radiation has been calculated based on the burial depth [35]. Total dose rates (Table 2) were calculated using DRAC v1.2 [36] taking into account attenuation due to moisture and grain size. An uncertainty of 2% has been added to the assigned water contents to account for variability during the burial period.

3.3. Documentary Flood Record

Documentary flood data were compiled to complement the palaeoflood data. Archival flood evidence provides direct (e.g., flood date, duration, stage or spatial extent) or indirect (e.g., post-flood damage repair) information of individual events, allowing flood chronologies and socio-economic

impacts to be analyzed [37,38]. Compilation of historical floods that occurred in the studied region was obtained mainly from scientific and technical reports, local history books and non-systematic compilations by historians Balbás Cruz [39], Fogues [40], Fontana [41], and from historical flood compilations by Beltrán Manrique [42], Sánchez-Adell et al. [43], and Camarasa and Segura [19]. Flood intensity was classified according to its basic hydrological behavior and the impacts on five categories following Barriendos et al. [37] classification: (1) Ordinary flood (non-overbank flood + disturbance); (2) Ordinary/extraordinary flood (Non-overbank flood + disturbance + damage); (3) Extraordinary flood (overbank flood + disturbance); (4) Extraordinary/catastrophic flood (Overbank flood + disturbance + damage), and (5) Catastrophic flood (Overbank flood + damage + destruction). A recent update of Mediterranean flood cases from documentary archives including our study region was published by Barriendos et al. [44].

3.4. Hydraulic Modelling

Palaeoflood discharge estimates follow from the assumption that the elevation of paleostage evidence (sediment layer) relates closely to the maximum stage attained by an identified flood [23]. Therefore, flood stages associated to the elevation of each flood unit in the stratigraphic profile were converted into discharge values. This conversion is an inverse problem, where the discharge is obtained by trial and error using hydraulic modelling by relating the surveyed elevation of the flood deposits to a simulated water surface profile [45].

The discharge estimation associated with the slackwater flood deposits was calculated using the US Army Corps of Engineers River Analysis System computer program-HEC-RAS [46]. The computation procedure is based on the solution of the one-dimensional energy equation, derived from the Bernoulli equation, for steady gradually varied flow. Therefore, the palaeoflood discharge is based on the calculation of a step-backwater profile producing the best correlation with the geological indicator of flow stage. A field survey was carried out in 2009 using a kinematic differential GPS Trimble 4700 with a precision of ± 1 cm in horizontal and ± 2 cm in vertical on real-time survey performance.

A total of 8 cross-sections were surveyed along a 1 km reach (Figure 1). Subcritical flow conditions were assumed along the reach, with critical flow selected as the boundary condition at the most downstream cross-section. Assigned Manning's n values were 0.03 for the valley floor and 0.04 for the valley margins. These n values were chosen according to our previous works in Rambla de la Viuda that used the Limerinos equation [47] for D_{50} and D_{84} grain sizes [20,48]. The hydraulic model was calibrated using field survey of high water marks of the December 2007 flood ($20 \text{ m}^3 \text{ s}^{-1}$). A sensitivity test performed on the model shows that for a 25% variation in roughness values, an error of 10–15% was introduced into the discharge results. Uncertainties in Manning's n values and energy loss coefficients had much less impact than uncertainties in cross-sectional data on discharge values estimated from hydraulic modelling [49].

Along the study reach, the potential channel incision, due to recent gravel mining in the channel, was estimated at one-meter average, based on field survey of gravel bars and channel remnants identified in the 1956 aerial photographs. As this channel bed degradation is due to gravel mining that took place from the 1980s, the discharge estimates of earlier floods are likely to overestimate the real peak flow in ca. 10%. However, as discharge estimates based on paleostage indicators represent a minimum discharge and assuming that slackwater deposition occurs within a water depth of 1–1.5 m, the estimated discharge may be close to real peak values. Individual flood layers overtopping the flood bench commonly increase in elevation into the valley side. Two discharge values were assigned to each flood set derived from modelled water surface profiles matching (1) the base of the alcove; and (2) the highest end-point of the flood sediments.

3.5. Frequency Analysis

Flood record stationarity for censored samples (systematic and palaeoflood) was confirmed using Lang's test [50]. This test assumes that stationary flood series can be described by a homogenous or

stationary Poisson process. The 95% tolerance interval of the accumulative number of floods above a threshold, or censored, level, is computed. Stationary flood series are those remaining within the 95% tolerance interval [51]. A flood frequency analysis was performed with the software PeakFQ [52] where systematic and non-systematic data are fit to a log-Pearson Type III distribution. The program applies a generalised method-of-moments estimator denoted the Expected Moments Algorithm (EMA [53]) and a generalised version of the Grubbs-Beck test for low outliers [54]. Visual matching to the calculated palaeoflood and systematic peaks plotting positions and the statistical parameters were used to test for goodness of fit.

4. Results

4.1. Uncertainties Affecting Flood Dating

Chronological control of the timing of the main stratigraphic packages was achieved by combined radiocarbon and OSL ages, and supported by documentary flood records. A most likely age was assigned to sedimentary units based on the combined intersection of luminescence and radiocarbon dating age range (e.g., highest probability of calibrated age ranges; Table 1) within a correct stratigraphic order. In some cases, it proved to be difficult to assign an unambiguous calendar age to individual flood events from ^{14}C and OSL dating. Post-Sixteenth century radiocarbon dating is affected by human influence on radiocarbon production (industrial and nuclear effects) which can make it difficult, in some cases, to assign a contemporary calendar age [55]. Regarding OSL dating, the dose distributions are characterized by large scatter with over-dispersion values $>80\%$, much higher than the 15% over-dispersion observed on the artificially bleached and irradiated subsample of MLL-17. Several authors applied descriptive and robust statistics to increase precision of the true burial dose of a population with incomplete bleaching grains [29,33,56,57]. Here, we applied the IEU minimum dose approach [33,34] which has successfully estimated ages for sequences of flood deposits in this region [29]. IEU identifies samples B1#3, B1 #4 and MLL #2 to be the ones with large (40–50%) population of well-bleached grains. In the remaining samples, only an average of $\sim 15\%$ of the *De* were identified to belong to well-bleached grains indicating a deficient exposition to light caused by reasons such as a short transport, high turbidity water or if the flood occurred at night. Estimating the equivalent doses from the population most likely to be well-bleached resulted in luminescence ages which are stratigraphically consistent (except sample MLL#17), although comparison with the radiocarbon ages still suggest a minor bias toward an overestimation of the burial dose.

4.2. Historical and Systematic Flood Records

The compiled documentary flood register from local historical chronicles (Castelló region) report a total of 400 large flood records since CE 1378. In the case of the Rambla de la Viuda and Montlleó rivers, the level of flood perception by its inhabitants was relatively low, mainly due to the location of major villages far from the river channel and flood areas. In addition, the river channel is entrenched in old alluvium, and the overflowing into urban settlements only occurs at the most downstream reaches, near the coast. Historical flood registers in this area report mainly about the damages caused on linear infrastructures crossing the channel such as irrigation canals, roads and bridges. According to the flood magnitude ranking (1 to 5) [37], most documented floods were classified within the extraordinary (level 3) to catastrophic (level 5) flood categories.

The analysis of regional documentary data (i.e., Millars River, Rambla de la Viuda, and other rivers at Castelló region) indicates an alternation of flood-rich and flood-poor periods over the last 500 years. The highest flood frequency occurred between 1580–1620, 1770–1810, 1880–1925, and 1945–1969. In contrast, periods between 1620–1770 and 1810–1880 were characterised by a high irregularity with few reported events or even absence of floods. In the Rambla de la Viuda river, seven large flood events were reported with category 5 over the period 1580–1900, namely in 1580, 1597, 1617, 1776, 1783,

1787, and 1883 (Figure 2). During the 20th century, large floods occurred in 1900, 1920, 1922, 1949, 1957, 1962, 1969 and 2000.

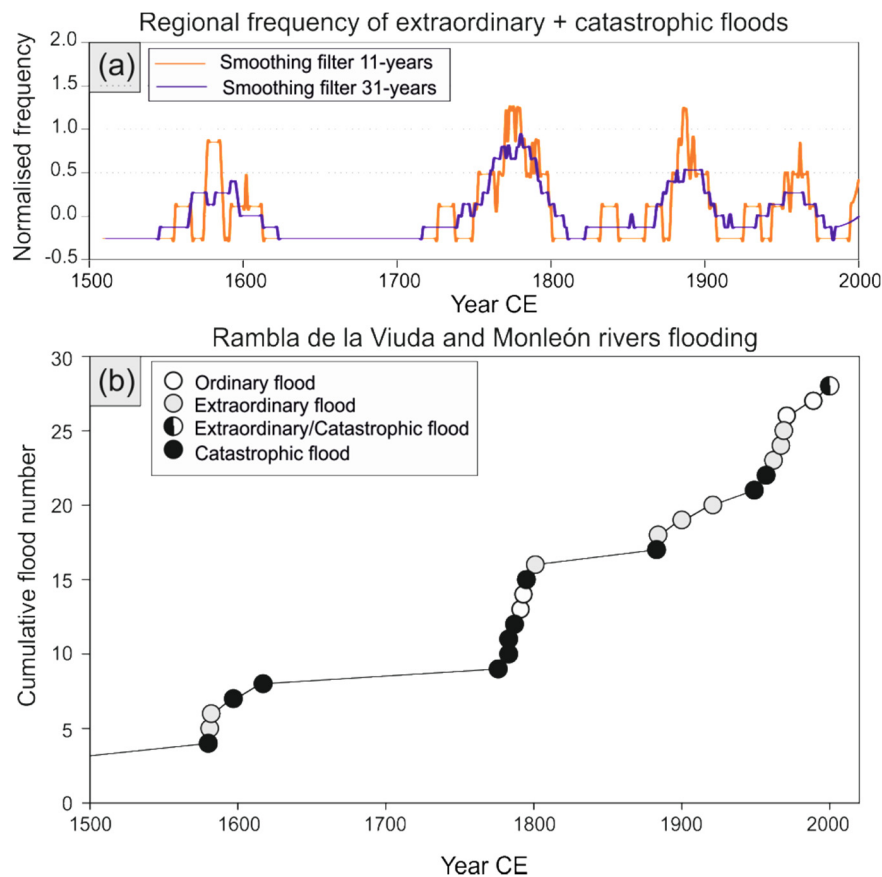


Figure 2. (a) Normalised annual flood series (this study) smoothed with a Gaussian filter (11 and 30 year, respectively) of extraordinary + catastrophic floods for the Castelló Province. The anomalies for AD 1500–1950 were estimated from documentary records, and after 1950 from instrumental data. Flood magnitude classification after Barriendos et al. [37]. (b) Accumulated number of documentary floods for Rambla de la Viuda and Montlleó rivers.

In the Montlleó River, continuous gauging began in 1971 at a station located 5 km upstream of the study area, and it is included in the Spanish Automatic Hydrological Information Systems (SAIH) network. The water authority provides, for this station, the daily mean discharge data. These daily discharge values were converted to peak discharges using the CEDEX approach [58] applied at regional level in the Júcar River basin, and modified in one parameter calibrated for Rambla de la Viuda catchment by Beneyto et al. [59] ($a = 82.86$ and $b = 0.51$). The longest gauged data record in the watershed (1956–2012) corresponds to the Rambla de la Viuda, and is based on the daily balance of water storage and release at the Maria Cristina Reservoir (construction started in 1910 and in operation since 1925). The largest gauged flood occurred on October 15, 1962 when the water overtopped the dam wall reaching according to the dam manager a peak flow of $1500 \text{ m}^3 \text{ s}^{-1}$ [60]. Since the construction of the Maria Cristina reservoir in 1920's, large floods exceeding the dam spillway ($600 \text{ m}^3 \text{ s}^{-1}$) occurred in 1920 (during the dam works), 1922, 1962, 1969 and 2000. The largest flood recorded by SAIH network (operative since 1988) occurred in year 2000 with a peak discharge of $1268 \text{ m}^3 \text{ s}^{-1}$ [61]. Epigraphic marks at the dam wall show that flood stage during the 1969 flood was halfway between 1962 and 2000 levels.

In the Montlleó River catchment, the largest reported flood occurred on the night of 9 October 1883 reaching ca. 6 m water stage in the small village of La Estrella. In this location, this heavy

rainfall produced a debris flow that destroyed 17 houses, damaged another 28 buildings, and caused 27 casualties (Newspaper El Liberal, 17 October 1883). Another extreme documented flood occurred in 1787 (October 8) in the nearby Alcora River (Rambla de la Viuda tributary) that destroyed the old Alcora dam built in 1580 ([62] cited in [63]).

4.3. Palaeoflood Hydrology

The stratigraphic profiles along the study reach are located in Figure 1d. Specific flood units discussed within the present work are referred to by the profile character identification (e.g., B1, MLL) and the flood unit number (unit #) indicated in the stratigraphic columns. Figure 3 presents information regarding flood sequences with characteristic lithofacies, sedimentary structures, and interpretation.

4.3.1. Flood Geomorphology and Sedimentology

Along the 6.5 km study reach, a lateral gravel bar was deposited on the river's eastern margin, attached to a terrace 6 m above the river thalweg (Figure 1d). This alluvial terrace is overlaid by flood sands and its surface shows traces of flooding, namely sand crevasse deposits. The stratigraphy in profiles B1 and B2 showed a similar number of flood events, 4 and 5 flood units respectively (Figure 4). The most complete stratigraphy (B2) accumulated a 1.1 m thick sequence with evidence of at least five flood units, with clear contacts marked by stone lines and bioturbation. The second lower unit consists of a medium sand trough cross-bedding structure indicative of high energy conditions (sequence PLT; Figure 3). Radiocarbon dating of the unit provided an age of cal. CE 1674–1894. The upper three units are composed of medium to fine sand within sequences of parallel lamination and climbing ripples in-drift, with indication of reverse flow direction (CR and PLR sequences). Profile B1 contains four units, the upper two are made of SWDs correlated to the B2 upper set, whereas the lower one comprises fluvial sands with OSL dates ~4000 years ago (Figure 4).

The best SWD outcrop is found within an alcove located on a 20-m cliff exposing Pleistocene gravels on the right valley side (circled A in Figure 1d). The alcove is filled with ca 5–6 m-thick slackwater flood deposits intercalated with layers of alluvial gravels and colluvium. The length of this remarkable outcrop (~14 m), together with additional transverse exposures dug across the alcove, provide a good three-dimensional composition of the SWD architecture (Figure 5). The frontal outcrop shows a complex flood stratigraphy due to its position on a valley side expansion, which creates a high energy eddy environment, and the recurrent input of gravelly hillslope colluvium often associated to periods of decreasing flood occurrence.

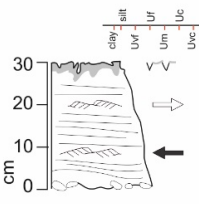
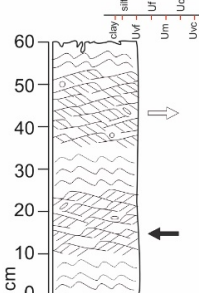
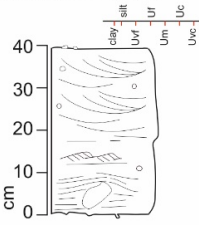
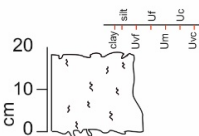
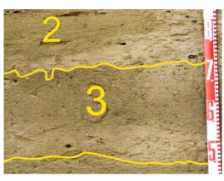
Sequence/Vertical log	Field Facies	Description	Interpretation
<p>PLR: Parallel-current ripples Thickness: 0.1-1m</p>  <p>E.g. Event # 6 MLI</p>	 <p>Detail of silt and clay laminae with desiccation cracks and bioturbation.</p>	<p>Fine to medium sand, parallel lamination and current ripples. Lower contacts by stone line or bioturbation. Some with basal parallel lamination adaptation to topography. Current ripples on the bottom or top of the sequence, with intercalated parallel lamination. Dominant ripples with reverse flow due to eddy flow. At the top, sequence grades to silt and clay laminae with desiccation cracks and bioturbation.</p>	<p>Vertical accretion made by plane beds migration when flood sand load and flow velocity increase or depth water decrease. Ripples represent changes in discharge, with a progressive decrease in velocity and flow transport. Alternating local current conditions result in ripple migration to plane bed migration if velocities increase or water depth laminae or grain size decrease. The grain size grade to silt when flow competence decreases until clay by settle down through a quasi-static suspension.</p>
<p>CR: Climbing ripples Thickness: 0.1-1m</p>  <p>E.g. Event #10 MLD</p>	 <p>Detail of climbing ripples.</p>	<p>Very fine to fine sand with clear contacts often marked by silt and/or clay laminar and/or bioturbation marks. Climbing ripples in-drift or in phase and parallel lamination either at the base or at the top of sequence. Climbing ripples with multiple flow directions (downstream and upstream or inner and outer alcove side). Sequence ends in silt-grained sand or mudstone thin laminae with desiccation cracks and bioturbation. Sequence 2 (MLI profile) out-of-phase upstream climbing ripples leading to in phase and these grade to out-of-phase downstream climbing ripples.</p>	<p>Deposited by sediment-laden water in excess of sand during ripples migration. Often during waning flow conditions with a decreasing in flow velocity and high rates of vertical build-up from suspension. High sediment load allows small granule to travel in suspension generating climbing ripples. Multiple flow direction indicative of a large eddy flow while backflow climbing; Sand excess dominant at peak flood discharge. Sequence 2 (MLI profile) interpreted as waning flow conditions with a decreasing in flow velocity that inhibits upstream vortices or due fluctuations in eddy axis.</p>
<p>PT: Parallel-Trough Thickness: 0.2-0.5 m</p>  <p>E.g. Event #4 B2 DR</p>	 <p>Detail parallel lamination adapting to wood rest.</p>	<p>Fine to medium sand with disperse granules. A clear base, often irregular, marked by stone lines or coarse sand and bioturbation overlain by parallel lamination, trough cross-bedding and sometimes current ripples.</p>	<p>Vertical accretion produced by migration of plane beds. Small 3D dunes developed as a response to flow variations during high discharge, with a progressive decrease in the velocity and in the capacity of transport of the current.</p>
<p>M: Massive Thickness: 0.2-0.35 m</p>  <p>E.g. Event #3 B3 DB</p>	 <p>View of massive sequence.</p>	<p>Medium sand to silty sand in massive sequences. No sedimentary structures or very diffuse lamination are observed.</p>	<p>Deposited by sediment-laden stream flow whose velocity sudden decrease in an ineffective flow area. Intense bioturbation due to vegetation and burrows made by annelids and arthropods partially deleted structures.</p>

Figure 3. Representative sedimentary sequences in the slackwater flood deposits of the Montlleó River, and interpretation of the sedimentary environment.

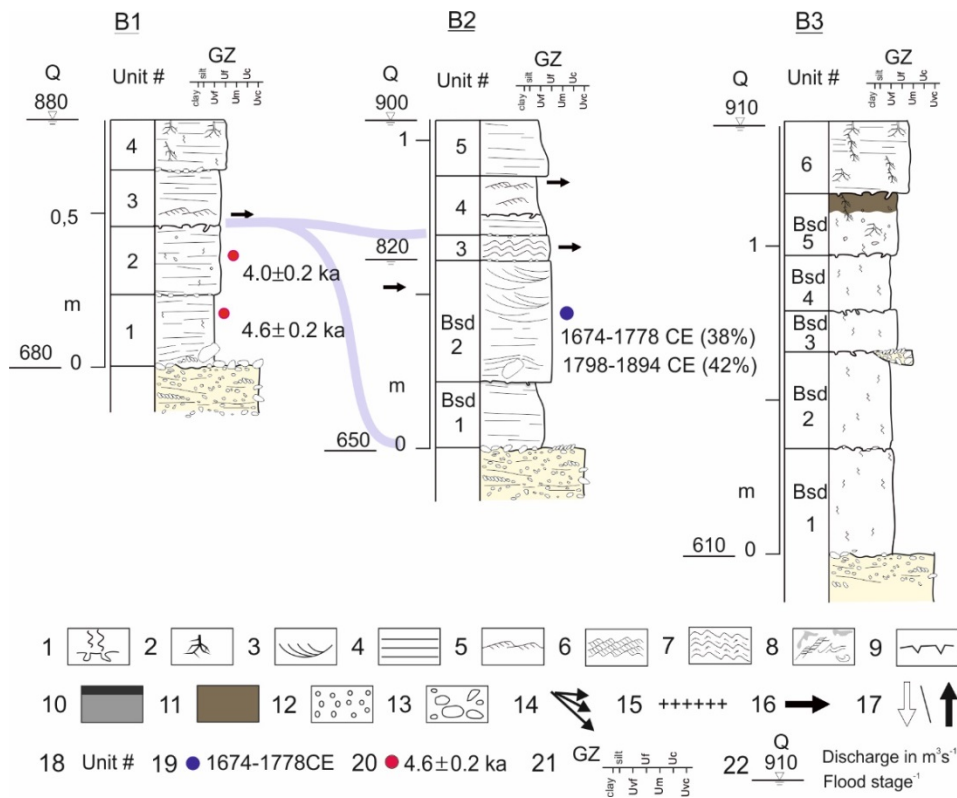


Figure 4. Stratigraphic profiles B1, B2 and B3 and proposed correlations. Radiocarbon dates in calibrated years (CE). Legend: 1: Bioturbation; 2: Root marks; 3: Planar (2d) cross bedding; 4: Parallel lamination; 5: Ripples; 6: climbing ripples; 7: Climbing ripples in phase; 8: Strong deformed and broken ripples; 9: mud cracks; 10: Soil (A horizon); 11: Silt and silty clay; 12: fluvial gravel; 13: Unsorted gravel (alluvial and colluvial); 14: Slope deposit; 15: Carbonate crust; 16: Reverse flow direction; 17: Inner and outer alcove flow directions; 18: Layer/sequence number; 19: Radiocarbon dating in calibrated years; 20: Luminescence dating in years before 2013; 21: Grain size (U: sand, Uvc: very coarse, Uc: coarse, Um: medium, Uf: fine, Uvf: very fine); 22: Discharge in $m^3 s^{-1}$ at marked stage.

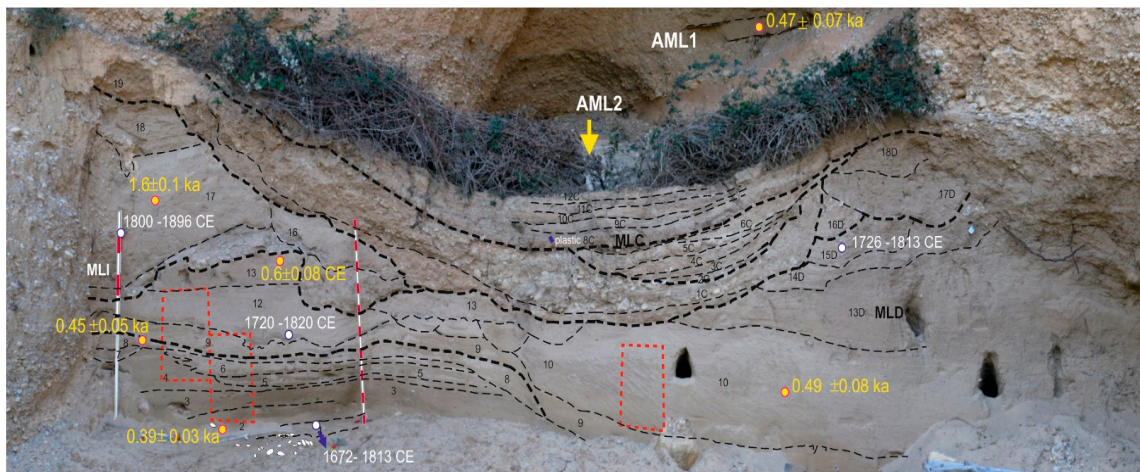


Figure 5. General view of the main alcove with indication of the stratigraphic units (fine dashed lines). Coarse dashed lines are contacts between the main stratigraphic packages. Most likely age range of calibrated Radiocarbon dating (white numbers) and luminescence dates results (yellow numbers) are indicated. AML1 and AM2 are inside the cave.

A composite stratigraphic sequence combining profile MLL and MLR shows at least 19 individual flood units within three SWD packages bound by sharp unconformities (Figure 6). Package I overlies fluvial gravels and comprises eight flood units (5–20-cm thick) made of very fine to fine sand (CR sequence; Figure 3) with clear contacts frequently marked by silt and/or clay laminar and/or bioturbation marks (burrows and/or root casts). Unit 1 yielded a radiocarbon age of cal CE 1672–1953 (Table 1), and units 2 and 8 were OSL dated to 0.39 ± 0.03 ka (CE 1595–1655) and 0.45 ± 0.05 ka (CE 1515–1615), respectively (Table 2).

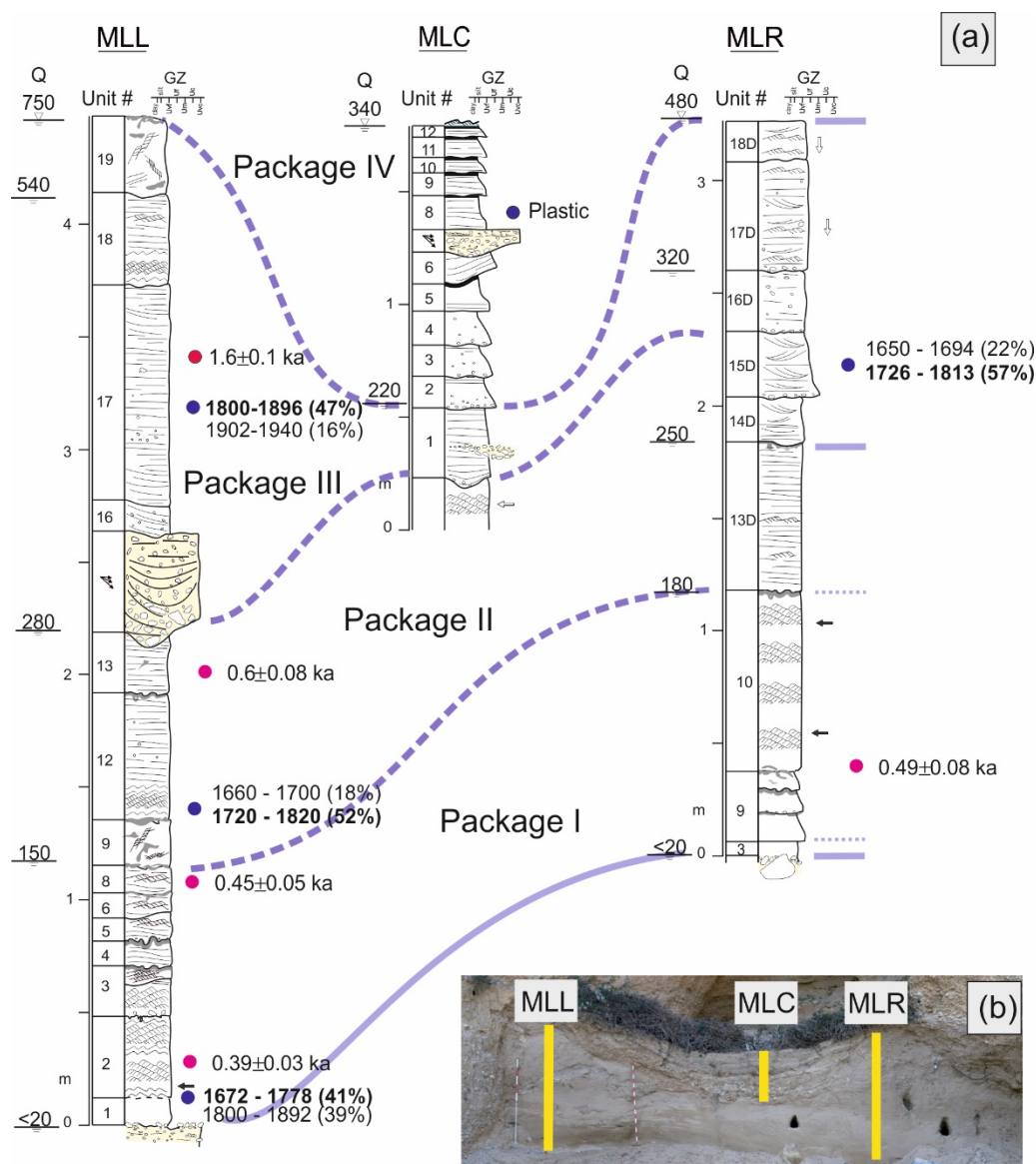


Figure 6. (a) Stratigraphic profiles MLL, MLC and MLR, and proposed correlations (dashed lines). Radiocarbon dates in calibrated years (CE) and luminescence dating in years before 2013. (b) The picture (same as Figure 5) shows the profile location. Legend in Figure 4.

Package II truncates and overtops package I. It is composed of seven flood units (units 9 to 15; Figure 6) that stack on a depression space at the downstream side of the alcove. In this set, unit 10 is the most prominent reaching ~1 m in thickness and consisting of fine sand with well-developed trains of climbing ripples with upstream flow direction indicative of a large eddy (sequence CR). OSL dating of unit 10 provided an age of 0.49 ± 0.08 ka (CE 1443–1603). Moreover, a sample at the base of unit 12

was radiocarbon dated to cal CE 1660–1953 (Table 1) and unit 13 was OSL dated to 0.6 ± 0.08 ka (CE 1333–1493; Table 2).

Package III (units 16 to 19) overlies a wedge of gravelly hillslope colluvium along the unconformity that truncates Package II (Figure 6). Its basal unit 17 is composed of a 1-m-thick sand layer with parallel lamination with occasional development of current ripples with downstream flow direction (sequence PLR). Radiocarbon dating of unit 15 provided an age of cal 1677–1940 whereas the OSL date resulted in 1.6 ± 0.1 ka (CE 313–513). This OSL date denotes a poor bleaching of the luminescence signal of the quartz grains. Package III was partially cut by gravel units and sands (Figure 5), most likely reworked from former flood deposits and coarse material that fell from the alcove walls.

A fourth SWD package (IV) overlies a 30-cm thick hillslope gravel unit that truncates most of package III (Figures 5 and 6). Package IV fills an erosion depression formed at the alcove entrance. Package IV flood units are described in profile MLC, showing two main flood depositional sets. The lower six units (MLC units 1 to 6; ~10 cm-thick each) consist of fine to medium sand with parallel lamination and reworked stone lines, mainly at the bottom part of the sequence. This lower set is overlain by hillslope colluvium of massive gravel that thin out towards the depression sides (Figure 5). The upper set consists of five units (MLC units 8 to 12; ~5–10 cm in thickness) composed of fine to very fine sand fining upward with parallel lamination, and silty clay laminae (Figure 6). The lowest unit contains a piece of green plastic indicating a recent age (likely post 1970s).

A cut trench inside AML2 exposes eight flood units overlying slope wash gravel (Figure 7), most likely equivalent to the gravel unit at the base of MLC. The basal units 6 and 7 are thicker and consist of fine sand with PLR type sequences culminated by silty clay laminae. Unit 7 was radiocarbon dated to cal CE 1690–1924 (Table 1). In the overlying units, no radiocarbon dates were obtained. However, these deposits are likely to correspond to 20th century floods like those in MLC.

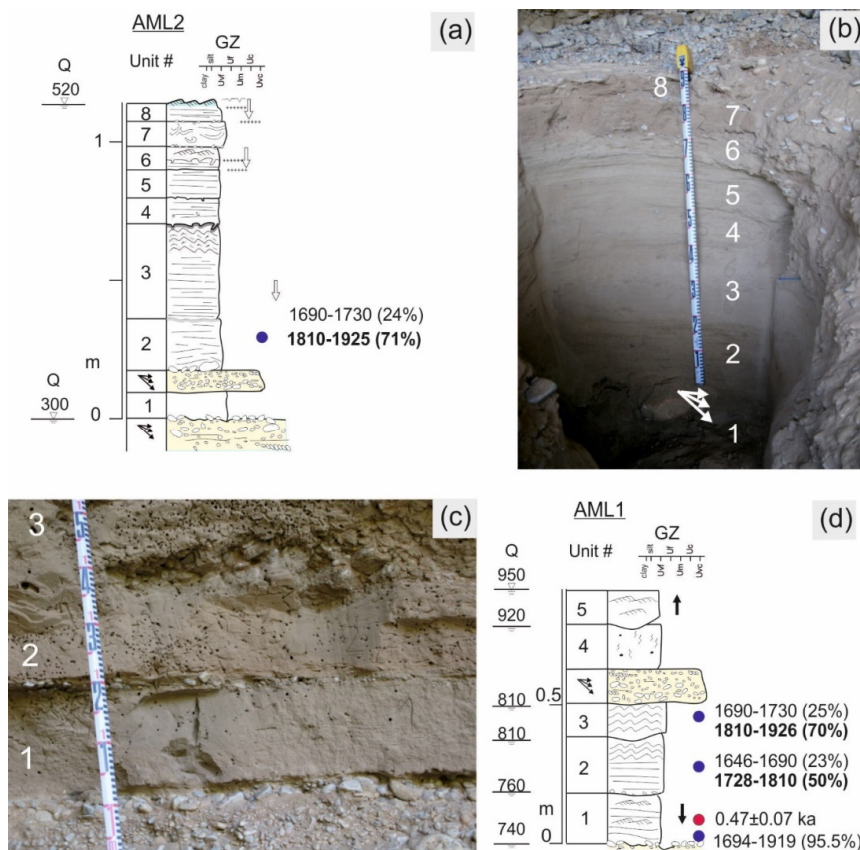


Figure 7. (a) Stratigraphic profile AML2 with indication of flood units and age dating results. (b) View of AML2 stratigraphy. (c) Stratigraphic log AML1. (d) View of AML1 profile.

On the right side of the alcove, there is evidence of a former SWDs fill, with pockets of flood stratigraphy preserved at the shelter wall at a higher elevation position (Figure 5). This stratigraphy (AML1; Figure 7) shows at least five flood units consisting of very fine sand with parallel lamination, ripples and climbing ripples in-phase with flow directions both towards the inner and outer alcove sides. Unit 1 was OSL dated to 0.47 ± 0.07 ka (CE 1475–1615; Table 2) and units 2 and 3 were radiocarbon dated cal CE 1646–1810 and cal CE 1690–1926, respectively (Table 1). In the upper section, two flood units are overlying a gravel bed. Although no dating material was found, the deposition of the upper flood unit could be attributed, considering their stratigraphical position and the documented flood records, to the 1962 flood, the largest in the 20th century flood record.

4.3.2. Discharge Estimation

Water surface profiles were calculated for multiple discharges related to the elevation of the slackwater flood deposits along the study reach. The step-backwater model results indicate that a discharge of $950 \text{ m}^3 \text{ s}^{-1}$ matches the highest palaeostage evidence corresponding to the alcove flood deposits in profile AML1. This profile AML1, located in the alcove interior, indicates that at least five floods exceeded a minimum discharge of $740\text{--}950 \text{ m}^3 \text{ s}^{-1}$ since year CE 1545. At the alcove cross-section, channel flow velocity was 4 ms^{-1} with subcritical flow conditions (Froude Number about 0.37). The model indicates a sharp velocity change from the channel to the alcove side where sediment was associated with eddy flow as reflected in the variable flow direction of the current ripples and the erosion pool created at the alcove entrance. Only inside the alcove was sedimentation associated with near stagnant water conditions.

The next highest discharge estimates are for profiles B1 and B2 and B3, overlying an alluvial terrace at the right valley side, with minimum discharge ranges of $680\text{--}880 \text{ m}^3 \text{ s}^{-1}$, $650\text{--}900 \text{ m}^3 \text{ s}^{-1}$ and $610\text{--}910 \text{ m}^3 \text{ s}^{-1}$, respectively. As indicated previously, profiles MLL and MLR at the alcove main deposit contains a record of at least 20 flood events since CE 1600. Hydraulic modelling resulted in minimum discharge estimates ranging from $>20 \text{ m}^3 \text{ s}^{-1}$ at the base of the outcrop, to $750 \text{ m}^3 \text{ s}^{-1}$ related to flood unit 17 at the top of profile MLL.

In the central part of the alcove, profiles MLC and AML1, containing flood evidence at least beginning in the 20th century provided minimum discharge ranges of 220 and $300 \text{ m}^3 \text{ s}^{-1}$, respectively. The flood unit 8 at profile MLC, that were found to contain plastic material, indicates that since the 1970s at least five floods exceeded a minimum discharge of $250 \text{ m}^3 \text{ s}^{-1}$. The uppermost flood units at both profiles MLC and AML1, indicate that the largest recent flood, the 2000 event, reached a minimum discharge of $500 \text{ m}^3 \text{ s}^{-1}$ in the study reach. This discharge is about three times the mean daily discharge recorded in Montlleó gauging station data.

4.4. Flood Frequency Analysis

Figure 8 illustrates the combined systematic and palaeoflood data used in the flood frequency analysis, where best-estimate ages are provided for the individual palaeofloods. Palaeoflood data provides information related to floods exceeding a given perception threshold in a period of known duration (Figure 8). The perception threshold is defined by the elevation of upper flood bed, therefore after deposition of each flood layer there is a self-rising of the minimum discharge threshold required to accumulate the next flood unit. Consequently, the exceedance probabilities of floods present on the stacked palaeoflood stratigraphy decrease as beds are built up. The sedimentary record is assumed to be complete for each flood exceeding the threshold of discharge at the palaeoflood site. Therefore, palaeoflood data can be treated as censored information, which can be handled efficiently by appropriate statistical methods [64,65].

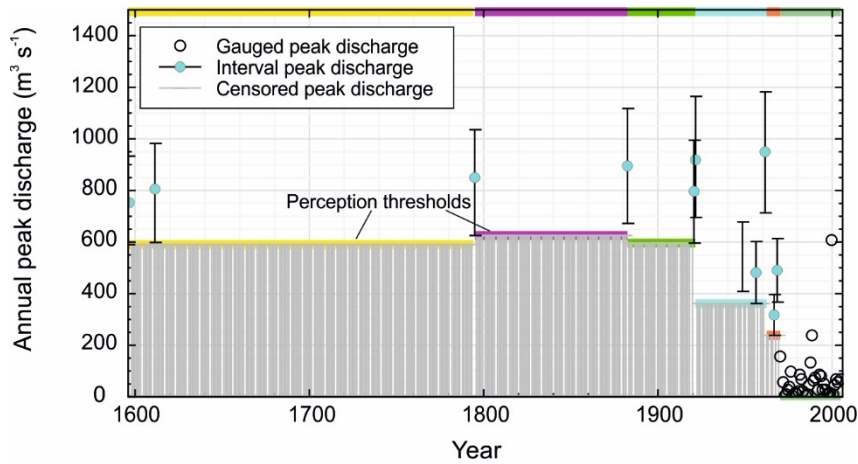


Figure 8. Schematic diagram showing discharges of palaeoflood, documentary and gauged floods. Grey shaded areas indicate censored flood records during the non-systematic period i.e., only floods exceeding in stage the top of the previous deposit were recorded. The blue dots show discharges for palaeoflood events $\pm 20\%$ discharge uncertainty (vertical lines). The white dots are annual flows from the Montlleó gauge station. For representation purposes, a tentatively palaeoflood age was assigned based on known flood years from documentary records.

Palaeoflood data from profiles AML1, B1 and B2, provided critical information regarding the largest palaeofloods (discharge and age) as lower bound data [66]. Moreover, their relative simple stratigraphy reduces the uncertainty of the missing of flood events exceeding the elevation of the depositional site. Additional palaeoflood information from other profiles (MLL, MLC and AML2) were incorporated as censored data or known flood discharges below threshold values.

Lang’s stationary test was passed for the palaeoflood and systematic records over the period CE 1590–2000, considering a threshold discharge above $450 \text{ m}^3 \text{ s}^{-1}$, (Figure 9). This confirms the assumption of stationarity in time (i.e., all floods were randomly generated from a single probability distribution with stable moments) for the use of statistical parametric models [50].

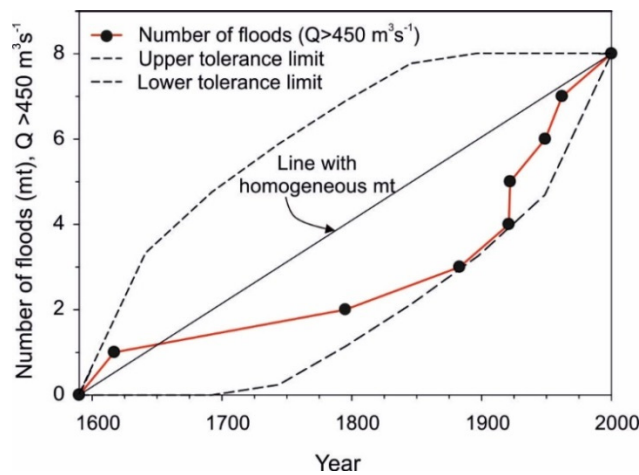


Figure 9. Stationary test on the time flood process at the Montlleó River over the period CE 1590–2000, for flood exceeding a discharge threshold of $450 \text{ m}^3 \text{ s}^{-1}$. The null hypothesis is to assume that the distribution of the number of exceedences can be described by a homogeneous Poisson process (i.e., independent and identically distributed random variables; [50]). The test is passed when the accumulated flood line (red line with black dots) stays inside the 90% tolerance interval (95 and 5% quantiles; dashed lines), implying the compliance of the Poisson process hypothesis.

Table 3 shows the peak discharge associated to different annual exceedance probabilities (return period) both with palaeoflood with systematic data and using only systematic record. Flood frequency analysis using palaeoflood data showed higher peak discharges than those obtained from the gauge record (Table 3). For instance, the calculated 1% annual probability flood (100-years average return interval) from combined palaeoflood and instrumental datasets is $710 \text{ m}^3 \text{ s}^{-1}$ whereas using only the systematic record is $460 \text{ m}^3 \text{ s}^{-1}$. In the case of the 1000-year flood, conventionally used for hydraulic design of infrastructures, frequency analysis with palaeoflood-gauge records show a discharge of $1525 \text{ m}^3 \text{ s}^{-1}$, whereas with only gauged data is $1020 \text{ m}^3 \text{ s}^{-1}$.

Table 3. Flood quantiles for different exceedance annual probabilities in Montlleó River (657 km²) and Rambla de la Viuda (1500 km²) fitted to, firstly, the annual maximum discharge of the systematic record only, and secondly to the combined systematic and palaeoflood discharges. The difference in % represents changes on flood probability introduced by climate variability related to “flood-rich” periods. Rambla de la Viuda frequency analysis for a two-component extreme value (TCEV) [20].

Annual Exceedance Probability (%)	Average Return Period (years)	Montlleó River			Rambla de la Viuda River		
		Discharge Syst. + paleo (m ³ s ⁻¹)	Discharge Systematic (m ³ s ⁻¹)	Change (%)	Discharge Syst. + paleo (m ³ s ⁻¹)	Discharge Systematic (m ³ s ⁻¹)	Change (%)
20	5	125	95	32	155	110	41
10	10	215	160	37	480	305	57
4	25	380	270	41	920	710	30
2	50	530	370	44	1250	1000	25
1	100	710	460	45	1570	1300	21
0.2	500	1240	840	48	2305	1975	17
0.1	1000	1525	1020	49	2615	2250	16

In Figure 10, the upper tail includes palaeofloods with discharge thresholds of $590\text{--}620 \text{ m}^3 \text{ s}^{-1}$, from which it is known were exceed 7 times in a period of 423 years, the last time being in year 2000. The plotting positions of the palaeoflood and gauged data information are within the confidence limits of the fitted distribution, an indication of a good fit. The low mean square error (MSE = 0.021) value also suggests a good consistency between the flood plotting positions (green dots in Figure 10) and the expected probability values. The oldest flood may correspond to the known catastrophic events of 1580, 1597 or 1616, the latest known as the year of diluvium [67].

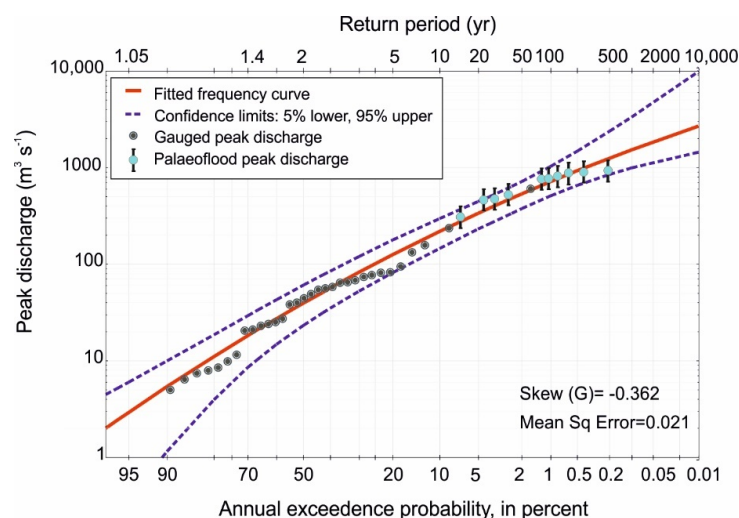


Figure 10. Log-Pearson 3 distribution fitted with systematic and palaeoflood data. Dots are plotting positions for the systematic (black dots) and palaeoflood records (blue dots with vertical lines).

5. Discussion

5.1. Information Content of Palaeoflood Data

The stratigraphic packages described in the main alcove, each comprising multiple SWD sequences, represent similar flood periods to those recorded in documentary sources. These flood deposit packages are bound by colluvial deposits corresponding to periods of lower flood frequency. The multiple insets of sedimentary bodies inside the alcove preserve a continuous record of the medium and large floods that occurred in the Montlleó River over the past 500 years.

The stratigraphy of the slackwater flood deposits discloses two main flood magnitude series. The first series contains the most complete SWD record corresponding to events of low to medium magnitude. It records up to 19 flood events representing floods with estimated minimum discharges between 20–750 m³ s⁻¹. An overlying inset, package IV (profile MLC), comprises of up to 12 flood layers with minimum estimated discharges between 220–340 m³ s⁻¹, most likely deposited over the last 100 years. The second flood series contains the stratigraphic evidence of the most extreme flood events, with estimated minimum discharges of between 740–950 m³ s⁻¹ and which extends back to CE 1540. The Montlleó slackwater flood deposits evidence of at least 5 flood events of this magnitude over this period (profile AML1), of which at least 2 flood events exceeded 850 m³ s⁻¹ in the last 200 years (profile B2). The palaeoflood hydrology of the Montlleó River contributes to a better understanding of flood discharges, as demonstrated when compared with the short-lived Montlleó gauge station record. Here the discharge of the year 2000 event, the largest in the gauge record, was recorded with a mean daily discharge of 129 m³ s⁻¹. Field evidence from high-elevation slackwater flood deposits of the 2000 event (AML2#8), identified by plastic and other human materials within the sediments, provide a minimum discharge of 520 m³ s⁻¹. The palaeoflood data analysis reveals the often insufficient quality of the gauged data in registering large flood events, and the added value of hydrological information obtained from the slackwater flood stratigraphy [11].

5.2. Palaeohydrology in the Climate and Environmental Context

The palaeoflood and documentary flood data presented show the alternation, during the past 500 years, of flood-rich and flood-poor periods involving both flood frequency and magnitude. A combined analysis of the information gathered from the documentary archives and from the palaeoflood sedimentary records made it possible to identify four flood cluster episodes: (1) 1570–1620 (Package I), (2) 1775–1795 (Package II), (3) 1850–1890 (Package III), and (4) 1920–1969 (lower set in Package IV). These flood-rich periods, lasting a few decades (30–50 years), are followed by a longer period characterised by a lack of flood deposits and dominated by slope washout sediment deposits within the stratigraphic profiles. These four flood periods correlate in time with others described elsewhere in the Mediterranean based on historical documentary evidence [44,68,69], lake records [70,71], and alluvial records [72,73].

Climatically, periods 1 and 3 correspond to cooler than usual (about 0.3 °C and 0.2 °C) climatic oscillations within the Little Ice Age (1300–1870) (cf. [44,74]). An accepted explanation is that heavy torrential rainfalls developed when anomalous cold air depressions come into contact with humid warm surficial air in the Mediterranean Sea. This type of Mediterranean cyclogenesis causes 75%–80% of the severe rainfall events in the area (mainly in autumn), the remainder being produced by winter-spring Atlantic fronts associated with zonal circulation [75]. Periods 1 and 3 also agree with decades of positive rainfall anomaly during both autumn (SON) and spring (MAM) and floods occurring during all seasons [76].

Period 2 comprises of a 20-years flood cluster at the end of the 18th century (large floods: 1776, 1783, 1787, 1795). This flood cluster coincides climatically with the “Malda Anomaly” (1760–1800) described for the Western Mediterranean as a period of high inter-annual hydrological variability (floods and droughts, [77]). In this high variability rainfall pattern, large floods occurred predominantly (>70%) in the autumn due to Mediterranean associated mesoscale convective systems [76]. A high frequency of

extreme rainfall indicates a predominant meridian circulation pattern (low index circulation) which it may lead to cut-off-low situations from the main westerly trough systems of cold air that often move along the Mediterranean Spanish coast [78].

Our palaeoflood record shows that the largest floods (e.g., 1581, 1597, 1617, 1783, 1787, 1883, 1962) occurred within periods of higher flood frequency, i.e., wetter than normal years. Machado et al. [76] describes that wet years produce higher spring and winter rainfalls, meaning that floods have secondary highs in winter or even spring or summer. In our Montlleó record, catastrophic and extraordinary floods occurred during autumn months (SON), whereas ordinary and a few extreme floods take place in winter and spring.

Large magnitude flooding over the late 18th century correlates in time with palaeovegetation and geochemical evidences important changes to land use (deforestation and grazing; [20]). The thick colluvium deposits, usually culminating in sequences of short-lived continuous slackwater flood units reflects drier climate conditions and intense land use changes, particularly the thick hillslope deposits overlying package III (Figure 5). Indeed, late 19th century coinciding with historical evidence of major economic and land-use changes (deforestation and increase in cultivated land in hillslopes; [79]).

5.3. Impacts of Global Change on Flood Frequency

The understanding of the causes of natural variability of flooding and their link to weather patterns and climate is essential for the assessment of the future changes of extreme events. Previous flood rich periods occurred during cooler and wetter climate conditions and only since the late 18th century flood clusters are often linked to periods with high inter-annual climatic variability (floods and droughts). Indeed, the frequency of continuous wetter phases has decreased since early 17th century, whereas the ones with marked annual variability have increased over the last 150 years [76]. Analysis of documentary records suggest a stationary long-term behaviour of high magnitude floods ($>300 \text{ m}^3 \text{ s}^{-1}$) over the last 500 years. Conversely, moderate-to-low magnitude events show a trend towards a reduction in frequency over the 20th and beginning of 21st century, in parallel with a reduction of annual maximum flow [8]. The reduction of mid-low discharge floods does not correlate with an equal negative trend on flood losses that rather show a general upward trend during the period 1971–2010, suggesting an increase on socio-economic vulnerability [80].

An important issue in hydrology is to define the risks of large floods. Conventional statistical analysis is usually restricted to a few dozen observations, which are used to estimate the probability of floods that exceed a chance of at least one in a hundred years. In this respect, palaeoflood data contains a wider range of climate variability impacts on flooding including situations of high hydrological variability exacerbated over the last 200 years. Hence, the impacts of climate variability on flood frequency can be evaluated comparing the flood quantiles resulting from analysis of gauged records with those extended by palaeoflood records. In the case of the Montlleó River, calculated flood quantiles (>50 years) from palaeoflood-gauged data shows 45%–50% higher discharges than those based only on instrumental data, the latter reflecting minor inter-decadal climate variability. Similar analysis for the Rambla de la Viuda catchment (1500 km^2), including the Montlleó River basin, shows a difference of 15–25% [20]. These results show a higher difference of flood discharge for a given quantile in smaller catchments, which is likely due to the limited extent of convective cells producing large floods.

The analysis of the palaeoflood record has revealed what flood magnitude is really possible over a long time frame that includes the effects of low-frequency climate variability in flooding. Flood quantile changes are, therefore, helpful indicators for understanding the impacts of climate variability on floods and for supporting adaptation to climate change. Our results, supported by scientific analysis, provide quantitative evaluation of flood change to assist in the decision of flood-risk management strategies and to identify low regret actions to cope with flooding [4]. As future flood projections are highly uncertain [1,3,6,7], the study of past extreme floods occurring during a full range of hydroclimatic variability allows a reliable assessment of flood hazards for a flexible adaptation to climate change.

6. Conclusions

The slackwater flood deposits (palaeofloods) and documentary flood archives of the Montlleó River (eastern Spain) provide evidence for extreme floods and their response to natural climate variability. The palaeoflood record identifies flood-rich and flood-poor episodes over the last 500 years. Four multi-decadal flood clusters were identified in the stratigraphic record, namely at periods 1: 1570–1620 (Package I), 2: 1775–1795 (Package II), 3: 1850–1890 (Package III), and 4: 1920–1969 (lower set in Package IV). Climatically, periods 1 and 3 were characterised by cooler than usual temperature (about 0.3 °C and 0.2 °C) during climatic oscillations of the Little Ice Age (1300–1870). However, periods 2 and 4 correspond to episodes of high inter-annual hydrological variability (floods and droughts) which became more frequent over the last hundred years. A direct consequence is the reduction of mid to low discharge floods over the 20th–early 21st century, which is also observed in the gauge record [8]. Conversely, our palaeoflood record shows a stationary long-term behaviour of high-magnitude floods ($>450 \text{ m}^3 \text{ s}^{-1}$) over the last 400 years. In the Montlleó River, at least five floods were recorded as high indicating minimum discharges of $740\text{--}950 \text{ m}^3 \text{ s}^{-1}$. This contrasts with the largest reported flood in year 2000, with a mean daily maximum discharge of $129 \text{ m}^3 \text{ s}^{-1}$. The impacts of flood probability changes induced by climate variability and change were weighed in relation to the catchment area size: the Montlleó River (657 km^2) and Rambla de la Viuda River (1500 km^2). In the case of the Montlleó River, calculated flood quantiles (>50 years) from palaeoflood-gauged data shows 45–50% higher discharges than those based only on instrumental data, the latter reflecting minor inter-decadal climate variability. Similar analysis for the Rambla de la Viuda catchment (1500 km^2), including the Montlleó River basin, shows a difference of 15–25%. These results show the higher difference of flood discharge for a given quantile in smaller catchments, which is likely due to the limited extent of mesoscale convective cells producing large floods. These findings have important implications for flood prevention, risk assessment and adaptation in small catchments of the Mediterranean region.

Author Contributions: G.B., Y.S.-M., A.S., M.R., M.J.M., A.M. and M.C. collected field data and interpreted the stratigraphic results. G.B., Y.S.-M. and M.J.M. wrote the first draft of the paper. M.B. collected and analysed the documentary flood database. A.M. performed the luminescence dating and wrote the methodological and OSL results sections of the paper. M.R. performed the hydraulic calculations. M.C., Y.S.-M. and G.B. designed and drew the figures. All authors interpreted results and contributed to framing and revising the paper. All authors have read and agreed to the published version of the manuscript.

Funding: This research was funded by the Ministry of Science, Innovation and Universities through the project “Assessment and modelling eco-hydrological and sedimentary responses in Mediterranean catchments for climate and environmental change adaptation” EPHIMED (CGL2017-86839-C3-1-R) co-financed with European FEDER funds.

Acknowledgments: The authors acknowledge that this study was supported by the project “Assessment and modelling eco-hydrological and sedimentary responses in Mediterranean catchments for climate and environmental change adaptation” EPHIMED (CGL2017-86839-C3-1-R) of the Ministry of Science, Innovation and Universities. This paper is a contribution of the Hydrology and Climate Change Laboratory (www.floodsresearch.com; twitter: floods_research; instagram: @floods_research).

Conflicts of Interest: The authors declare no potential conflict of interest.

References

1. Jiménez Cisneros, B.E.; Oki, T.; Arnell, N.W.; Benito, G.; Cogley, J.G.; Döll, P.; Jiang, T.; Mwakalila, S.S. Freshwater Resources. In *Climate Change 2014—Impacts, Adaptation and Vulnerability: Part A: Global and Sectoral Aspects: Working Group II Contribution to the IPCC Fifth Assessment Report: Volume 1: Global and Sectoral Aspects*; Field, C.B., Barros, V.R., Dokken, D.J., Mach, K.J., Mastrandrea, M.D., Bilir, T.E., Chatterjee, M., Ebi, K.L., Estrada, Y.O., Genova, R.C., et al., Eds.; Cambridge University Press: Cambridge, UK; New York, NY, USA, 2014; Volume 1, pp. 229–270.
2. Redmond, K.T.; Enzel, Y.; House, P.K.; Biondi, F. Climate variability and flood frequency at decadal to millennial time scales. In *Ancient Floods, Modern Hazards. Principles and Applications of Paleoflood Hydrology*; House, P.K., Webb, R.H., Baker, V.R., Levish, D.R., Eds.; Water Science and Application Series; American Geophysical Union: Washington, DC, USA, 2002; pp. 21–45.

3. Kundzewicz, Z.W.; Kanae, S.; Seneviratne, S.I.; Handmer, J.; Nicholls, N.; Peduzzi, P.; Mechler, R.; Bouwer, L.M.; Arnell, N.; Mach, K.; et al. Flood risk and climate change: Global and regional perspectives. *Hydrol. Sci. J.* **2013**, *59*, 1–28. [[CrossRef](#)]
4. Döll, P.; Jiménez-Cisneros, B.; Oki, T.; Arnell, N.W.; Benito, G.; Cogley, J.G.; Jiang, T.; Kundzewicz, Z.W.; Mwakalila, S.; Nishijima, A. Integrating risks of climate change into water management. *Hydrol. Sci. J.* **2014**, *60*, 4–13. [[CrossRef](#)]
5. Monjo, R.; Gaitán, E.; Pórtoles, J.; Ribalaygua, J.; Torres, L. Changes in extreme precipitation over Spain using statistical downscaling of CMIP5 projections. *Int. J. Climatol.* **2016**, *36*, 757–769. [[CrossRef](#)]
6. Garijo, C.; Mediero, L. Assessment of Changes in Annual Maximum Precipitations in the Iberian Peninsula under Climate Change. *Water* **2019**, *11*, 2375. [[CrossRef](#)]
7. Alfieri, L.; Burek, P.; Feyen, L.; Forzieri, G. Global warming increases the frequency of river floods in Europe. *Hydrol. Earth Syst. Sci.* **2015**, *19*, 2247–2260. [[CrossRef](#)]
8. Mediero, L.; Santillán, D.; Garrote, L.; Granados, A. Detection and attribution of trends in magnitude, frequency and timing of floods in Spain. *J. Hydrol.* **2014**, *517*, 1072–1088. [[CrossRef](#)]
9. Blöschl, G.; Hall, J.; Parajka, J.; Perdigão, R.A.P.; Merz, B.; Arheimer, B.; Aronica, G.T.; Bilibashi, A.; Bonacci, O.; Borga, M.; et al. Changing climate shifts timing of European floods. *Science* **2017**, *357*, 588–590. [[CrossRef](#)]
10. Rodríguez-Lloveras, X.; Buytaert, W.; Benito, G. Land use can offset climate change induced increases in erosion in Mediterranean watersheds. *Catena* **2016**, *143*, 244–255. [[CrossRef](#)]
11. Baker, V.R. Paleoflood hydrology: Origin, progress, prospects. *Geomorphology* **2008**, *101*, 1–13. [[CrossRef](#)]
12. Benito, G.; Thorndycraft, V.R. Palaeoflood hydrology and its role in applied hydrological sciences. *J. Hydrol.* **2005**, *313*, 3–15. [[CrossRef](#)]
13. Baker, V.R.; Kochel, R.C. Flood sedimentation in bedrock fluvial systems. In *Flood Geomorphology*; Baker, V.R., Kochel, R.C., Patton, P.C., Eds.; John Wiley & Sons, Ltd.: New York, NY, USA, 1988; pp. 123–137.
14. Ely, L.L.; Enzel, Y.; Baker, V.R.; Cayan, D.R. A 5000-year record of extreme floods and climate change in the southwestern United States. *Science* **1993**, *262*, 410–412. [[CrossRef](#)] [[PubMed](#)]
15. Ballesteros-Canovas, J.; Stoffel, M.; Benito, G.; Rohrer, M.; Barriopedro, D.; García-Herrera, R.; Beniston, M.; Brönnimann, S. On the extraordinary winter flood episode over the North Atlantic Basin in 1936. *Ann. N. Y. Acad. Sci.* **2019**, *1436*, 206–216. [[CrossRef](#)] [[PubMed](#)]
16. Rodríguez-Lloveras, X.; Corella, J.P.; Benito, G. Modelling the Hydro-Sedimentary Dynamics of a Mediterranean Semiarid Ungauged Watershed Beyond the Instrumental Period. *Land Degrad. Dev.* **2017**, *28*, 1506–1518. [[CrossRef](#)]
17. Corella, J.P.; Benito, G.; Wilhelm, B.; Montoya, E.; Rull, V.; Vegas-Vilarrúbia, T.; Valero-Garcés, B.L. A millennium-long perspective of flood-related seasonal sediment yield in Mediterranean watersheds. *Glob. Planet. Chang.* **2019**, *177*, 127–140. [[CrossRef](#)]
18. Mateu, J.F. La Rambla de la Viuda. Clima e hidrología. *Cuad. Geogr.* **1974**, *15*, 47–68.
19. Camarasa, A.M.; Segura, F. Flood events in Mediterranean ephemeral streams (ramblas) in Valencia region, Spain. *Catena* **2001**, *45*, 229–249. [[CrossRef](#)]
20. Machado, M.J.; Medialdea, A.; Calle, M.; Rico, M.T.; Sánchez-Moya, Y.; Sopena, A.; Benito, G. Historical palaeohydrology and landscape resilience of a Mediterranean rambla (Castellón, NE Spain): Floods and people. *Quat. Sci. Rev.* **2017**, *171*, 182–198. [[CrossRef](#)]
21. Calle, M.; Alho, P.; Benito, G. Channel dynamics and geomorphic resilience in an ephemeral Mediterranean river affected by gravel mining. *Geomorphology* **2017**, *285*, 333–346. [[CrossRef](#)]
22. Calle, M.; Calle, J.; Alho, P.; Benito, G. Inferring sediment transfers and functional connectivity of rivers from repeat topographic surveys. *Earth Surf. Process. Landf.* **2020**, *45*, 681–693. [[CrossRef](#)]
23. Benito, G.; O'Connor, J.E. Quantitative Paleoflood Hydrology. In *Treatise on Geomorphology*; Shroder, J.F., Wohl, E., Eds.; Academic Press: San Diego, CA, USA, 2013; Volume 9, pp. 459–474.
24. Benito, G.; Sánchez-Moya, Y.; Sopena, A. Sedimentology of high-stage flood deposits of the Tagus River, Central Spain. *Sediment. Geol.* **2003**, *157*, 107–132. [[CrossRef](#)]
25. Thorndycraft, V.R.; Benito, G.; Rico, M.; Sopena, A.; Sanchez-Moya, Y.; Casas, A. A long-term flood discharge record derived from slackwater flood deposits of the Llobregat River, NE Spain. *J. Hydrol.* **2005**, *313*, 16–31. [[CrossRef](#)]
26. Ramsey, C.B. Development of the Radiocarbon Program OxCal. *Radiocarbon* **2001**, *43*, 355–363. [[CrossRef](#)]

27. Reimer, P.J.; Bard, E.; Bayliss, A.; Beck, J.W.; Blackwell, P.G.; Ramsey, C.B.; Buck, C.E.; Cheng, H.; Edwards, R.L.; Friedrich, M.; et al. IntCal13 and Marine13 Radiocarbon Age Calibration Curves 0–50,000 Years cal BP. *Radiocarbon* **2013**, *55*, 1869–1887. [[CrossRef](#)]
28. Aitken, M.J. *An Introduction to Optical Dating. The Dating of Quaternary Sediments by the Use of Photon-Stimulated Luminescence*; Oxford University Press: Oxford, UK, 1998; p. 267.
29. Medialdea, A.; Thomsen, K.J.; Murray, A.S.; Benito, G. Reliability of equivalent-dose determination and age-models in the OSL dating of historical and modern palaeoflood sediments. *Quat. Geochronol.* **2014**, *22*, 11–24. [[CrossRef](#)]
30. Truelsen, J.; Wallinga, J. Zeroing of the OSL signal as a function of grain size: Investigating bleaching and thermal transfer for a young fluvial sample. *Geochronometria* **2003**, *22*, e8.
31. Murray, A.S.; Wintle, A.G. Luminescence dating of quartz using an improved single-aliquot regenerative-dose protocol. *Radiat. Meas.* **2000**, *32*, 57–73. [[CrossRef](#)]
32. Duller, G.A.T. Distinguishing quartz and feldspar in single grain luminescence measurements. *Radiat. Meas.* **2003**, *37*, 161–165. [[CrossRef](#)]
33. Thomsen, K.J.; Jain, M.; Bøtter-Jensen, L.; Murray, A.S.; Jungner, H. Variation with depth of dose distributions in single grains of quartz extracted from an irradiated concrete block. *Radiat. Meas.* **2003**, *37*, 315–321. [[CrossRef](#)]
34. Thomsen, K.J.; Murray, A.S.; Bøtter-Jensen, L.; Kinahan, J. Determination of burial dose in incompletely bleached fluvial samples using single grains of quartz. *Radiat. Meas.* **2007**, *42*, 370–379. [[CrossRef](#)]
35. Prescott, J.R.; Hutton, J.T. Cosmic ray contributions to dose rates for luminescence and ESR dating: Large depths and long-term time variations. *Radiat. Meas.* **1994**, *23*, 497–500. [[CrossRef](#)]
36. Durcan, J.A.; King, G.E.; Duller, G.A.T. DRAC: Dose Rate and Age Calculator for trapped charge dating. *Quat. Geochronol.* **2015**, *28*, 54–61. [[CrossRef](#)]
37. Barriendos, M.; Ruiz-Bellet, J.; Tuset, J.; Bueso, J.; Balasch, J.; Pino Gonzalez, D.; Ayala, J. The “Prediflood” database of historical floods in Catalonia (NE Iberian Peninsula) AD 1035–2013, and its potential applications in flood analysis. *Hydrol. Earth Syst. Sci.* **2014**, *18*, 4807–4823. [[CrossRef](#)]
38. Brázdil, R.; Kundzewicz, Z.W.; Benito, G. Historical hydrology for studying flood risk in Europe. *Hydrol. Sci. J. - J. Des Sci. Hydrol.* **2006**, *51*, 739–764. [[CrossRef](#)]
39. Balbás Cruz, J.A. *El libro de la provincial de Castellón*; Imprenta y librería de J. Armengot: Castellón, Spain, 1892.
40. Fogues, F. Las inundaciones de la Ribera. *An. Del Cent. De Cult. Valencia.* **1931**, *4*, 232–250.
41. Fontana, J.M. Historia del clima en el litoral mediterráneo: Reino de Valencia más provincia de Murcia. Unpublished report, Jávea. 1978.
42. Beltrán Manrique, E. *Almanzora. El Mijares. Narración Histórica*; Armengot: Castellón, Spain, 1958.
43. Sánchez-Adell, J.; Olcina, F.; Sánchez-Almela, E. *Elenco de Fechas Para la Historia Urbana de Castellón de la Plana*; Soc. Castellonense de Cultura: Castellón, Spain, 1993.
44. Barriendos, M.; Gil-Guirado, S.; Pino, D.; Tuset, J.; Pérez-Morales, A.; Alberola, A.; Costa, J.; Balasch, J.C.; Castelltort, X.; Mazón, J.; et al. Climatic and social factors behind the Spanish Mediterranean flood event chronologies from documentary sources (14th–20th centuries). *Glob. Planet. Chang.* **2019**, *182*, 102997. [[CrossRef](#)]
45. Benito, G.; Lang, M.; Barriendos, M.; Llasat, M.C.; Francés, F.; Ouarda, T.; Thorndycraft, V.R.; Enzel, Y.; Bardossy, A.; Coeur, D.; et al. Use of systematic, palaeoflood and historical data for the improvement of flood risk estimation. Review of scientific method. *Nat. Hazards* **2004**, *31*, 623–643.
46. Hydrologic Engineering Center. *HEC-RAS, River Analysis System, Hydraulics Version 4.1. Reference Manual, (CPD-69)*; U.S. Army Corps of Engineers: Davis, CA, USA, 2010; p. 411.
47. Limerinos, J.T. *Determination of the Manning Coefficient from Measured Bed Roughness in Natural Channels*; Geological Survey Water-Supply paper 1898-B; US Geological Survey: Washington, DC, USA, 1970.
48. Lotsari, E.S.; Calle, M.; Benito, G.; Kukko, A.; Kaartinen, H.; Hyyppä, J.; Hyyppä, H.; Alho, P. Topographical change caused by moderate and small floods in a gravel bed ephemeral river—A depth-averaged morphodynamic simulation approach. *Earth Surf. Dyn.* **2018**, *6*, 163–185. [[CrossRef](#)]
49. O’Connor, J.E.; Webb, R.H. Hydraulic modeling for paleoflood analysis. In *Flood Geomorphology*; Baker, V.R., Kochel, R.C., Patton, P.C., Eds.; John Wiley & Sons: New York, NY, USA, 1988; pp. 393–402.
50. Lang, M.; Ouarda, T.B.M.J.; Bobée, B. Towards operational guidelines for over-threshold modeling. *J. Hydrol.* **1999**, *225*, 103–117. [[CrossRef](#)]

51. Nautlet, R.; Lang, M.; Ouarda, T.; Coeur, D.; Bobee, B.; Recking, A.; Moussay, D. Flood frequency analysis on the Ardeche river using French documentary sources from the last two centuries. *J. Hydrol.* **2005**, *313*, 58–78. [[CrossRef](#)]
52. Veilleux, A.G.; Cohn, T.A.; Flynn, K.M.; Mason, R.R., Jr.; Hummel, P.R. *Estimating Magnitude and Frequency of Floods Using the PeakFQ 7.0 Program (2013-3108)*; US Geological Survey: Reston, VA, USA, 2014.
53. Cohn, T.A.; Lane, W.L.; Baier, W.G. An algorithm for computing moments-based flood quantile estimates when historical flood information is available. *Water Resour. Res.* **1997**, *33*, 2089–2096. [[CrossRef](#)]
54. Cohn, T.A.; England, J.F.; Berenbrock, C.E.; Mason, R.R.; Stedinger, J.R.; Lamontagne, J.R. A generalized Grubbs-Beck test statistic for detecting multiple potentially influential low outliers in flood series. *Water Resour. Res.* **2013**, *49*, 5047–5058. [[CrossRef](#)]
55. Taylor, R.; Bar-Yosef, O. *Radiocarbon Dating*; Routledge: New York, NY, USA, 2014.
56. Galbraith, R.F. *Statistics for Fission Track Analysis*; Chapman and Hall/CRC: Boca Raton, FL, USA, 2005.
57. Arnold, L.J.; Roberts, R.G.; Galbraith, R.F.; DeLong, S.B. A revised burial dose estimation procedure for optical dating of young and modern-age sediments. *Quat. Geochronol.* **2009**, *4*, 306–325. [[CrossRef](#)]
58. CEDEX. *Mapa de Caudales Máximos. Memoria Técnica*; Ministerio de Medioambiente y Medio Rural y Marino: Madrid, Spain, 2011.
59. Beneyto, C.; Aranda, J.A.; Benito, G.; Francés, F. Metodología basada en generadores meteorológicos para la estimación de avenidas extremas. *Ing. Agua* **2019**, *23*, 259–273. [[CrossRef](#)]
60. Mateu, J.F. *La Primera Confederación Hidrográfica del Júcar (1934–1942)*; Valencia, Confederación Hidrográfica del Júcar: Valencia, Spain, 2010.
61. Gabaldó, O.; Fleitz, J.; Villalba Bergado, F. SAIH Flood warning system and emergency management in the Júcar basin (Spain): The case study of October 2000. In Proceedings of the Mitigation of Climate Induced Natural Hazards (MITCH) Workshop II: Advances in Flood Forecasting, Barcelona, Spain, 10–12 June 2002; Flood Warning and Emergency Management: Barcelona, Spain, 2002; p. 15.
62. Cavanilles, A.J. *Observaciones Sobre la Historia Natural, Geografía del Reyno de Valencia*. Imprenta Real. Madrid; Reproducción Facsímil, Ediciones Albatros: Valencia, Spain, 1985; Volume 2, pp. 1795–1797.
63. López-Gómez, A. Presas y canales de riego en los siglos XVI y XVII. In *Hitos Históricos de los Regadíos Españoles*; Gil Olcina, A., Morales Gil, A., Eds.; Ministerio de Agricultura, Pesca y Alimentación: Madrid, Spain, 1992; pp. 91–142.
64. Stedinger, J.R.; Cohn, T.A. Flood frequency analysis with historical and paleoflood information. *Water Resour. Res.* **1986**, *22*, 785–793. [[CrossRef](#)]
65. Frances, F.; Salas, J.D.; Boes, D.C. Flood frequency-analysis with systematic and historical or paleoflood data-based on the 2-parameter General Extreme-Value models. *Water Resour. Res.* **1994**, *30*, 1653–1664. [[CrossRef](#)]
66. Botero, B.A.; Francés, F. Estimation of high return period flood quantiles using additional non-systematic information with upper bounded statistical models. *Hydrol. Earth Syst. Sci.* **2010**, *14*, 2617–2628. [[CrossRef](#)]
67. Thorndycraft, V.R.; Barriendos, M.; Benito, G.; Rico, M.; Casas, A. The catastrophic floods of AD 1617 in Catalonia (northeast Spain) and their climatic context. *Hydrol. Sci. J.* **2006**, *51*, 899–912. [[CrossRef](#)]
68. Barriendos, M.; Martín-Vide, J. Secular Climatic Oscillations as Indicated by Catastrophic Floods in the Spanish Mediterranean Coastal Area (14th–19th Centuries). *Clim. Chang.* **1998**, *38*, 473–491.
69. Llasat, M.-C.; Barriendos, M.; Barrera, A.; Rigo, T. Floods in Catalonia (NE Spain) since the 14th century. Climatological and meteorological aspects from historical documentary sources and old instrumental records. *J. Hydrol.* **2005**, *313*, 32–47. [[CrossRef](#)]
70. Corella, J.P.; Benito, G.; Rodríguez-Lloveras, X.; Brauer, A.; Valero-Garcés, B.L. Annually-resolved lake record of extreme hydro-meteorological events since AD 1347 in NE Iberian Peninsula. *Quat. Sci. Rev.* **2014**, *93*, 77–90. [[CrossRef](#)]
71. Corella, J.P.; Valero-Garcés, B.L.; Vicente-Serrano, S.M.; Brauer, A.; Benito, G. Three millennia of heavy rainfalls in Western Mediterranean: Frequency, seasonality and atmospheric drivers. *Sci. Rep.* **2016**, *6*, 38206. [[CrossRef](#)] [[PubMed](#)]
72. Benito, G.; Macklin, M.G.; Zielhofer, C.; Jones, A.F.; Machado, M.J. Holocene flooding and climate change in the Mediterranean. *Catena* **2015**, *130*, 13–33. [[CrossRef](#)]

73. Benito, G.; Macklin, M.G.; Panin, A.; Rossato, S.; Fontana, A.; Jones, A.F.; Machado, M.J.; Matlakhova, E.; Mozzi, P.; Zielhofer, C. Recurring flood distribution patterns related to short-term Holocene climatic variability. *Sci. Rep.* **2015**, *5*, 16398. [[CrossRef](#)] [[PubMed](#)]
74. Blöschl, G.; Kiss, A.; Viglione, A.; Barriendos, M.; Böhm, O.; Brázdil, R.; Coeur, D.; Demarée, G.; Llasat, M.C.; Macdonald, N.; et al. Current flood-rich period is exceptional compared to the past 500 years in Europe. *Nature* **2020**. in review.
75. Millán, M.M. Extreme hydrometeorological events and climate change predictions in Europe. *J. Hydrol.* **2014**, *518*, 206–224. [[CrossRef](#)]
76. Machado, M.J.; Benito, G.; Barriendos, M.; Rodrigo, F.S. 500 Years of rainfall variability and extreme hydrological events in southeastern Spain drylands. *J. Arid Environ.* **2011**, *75*, 1244–1253. [[CrossRef](#)]
77. Barriendos, M.; Llasat, M.C. The case of the ‘Maldá’ anomaly in the Western Mediterranean basin (AD 1760–1800): An example of a strong climatic variability. *Clim. Chang.* **2003**, *61*, 191–216. [[CrossRef](#)]
78. Capel Molina, J. Génesis de las inundaciones de Octubre de 1973 en el Sureste de la Península Ibérica. *Cuad. Geográficos* **1974**, *4*, 149–166.
79. Benito, G.; Rico, M.; Sánchez-Moya, Y.; Sopena, A.; Thorndycraft, V.R.; Barriendos, M. The impact of late Holocene climatic variability and land use change on the flood hydrology of the Guadalentín River, southeast Spain. *Glob. Planet. Chang.* **2010**, *70*, 53–63. [[CrossRef](#)]
80. Benito, G.; Machado, M.J. Floods in the Iberian Peninsula. In *Changes of Flood Risk in Europe*; Kundzewicz, Z.W., Ed.; IAHS Press and CRC Press/Balkema: Wallingford, Oxfordshire, UK, 2012; pp. 372–383. [[CrossRef](#)]



© 2020 by the authors. Licensee MDPI, Basel, Switzerland. This article is an open access article distributed under the terms and conditions of the Creative Commons Attribution (CC BY) license (<http://creativecommons.org/licenses/by/4.0/>).